

Macroscopic localization and collective memory in Poisson renewal resetting

Ohad Vilk^{1,*}

¹*Racah Institute of Physics, Hebrew University of Jerusalem, Jerusalem 91904, Israel*

Stochastic renewal processes are ubiquitous across physics, biology, and the social sciences. Here, we show that continuous-time renewal dynamics can naturally produce a mixed discrete-continuous structure, with a macroscopic fraction of particles occupying a discrete state. For ensembles of continuous-time random walkers subject to Poissonian renewal resets, we develop an age-structured framework showing this discrete component corresponds to localization at the reset configuration. We next show that collective interactions can retain memory although all reset events are memoryless. Remarkably, the transition to collective memory is discontinuous, and we identify a first-order dynamical phase transition between weak collective bias, where the dynamics are stationary, to strong collective bias where the dynamics are nonstationary and display aging up to finite-size effects. We explicitly discuss ecological implications of our work, illustrating how continuous-time renewal dynamics shape macroscopic structure and collective organization with long-term memory.

Many systems exhibit long-term memory, manifested by slow, history-dependent relaxation of macroscopic observables. Examples include intermittently emitting quantum dots, neuronal activity with bursty temporal dynamics, and human or animal movement [1–10]. A predominant theoretical approach to describe such *aging* behavior is based on non-Poissonian renewal processes, where broadly distributed waiting times lead to a decaying renewal rate, and observables depend explicitly on the time since system preparation [11–13]. A paradigmatic realization is provided by the continuous-time random walk (CTRW), in which stochastic motion is interspersed by power-law waiting times, giving rise to anomalous transport and aging [14–16]. By contrast, Poisson renewal processes provide a memoryless benchmark.

In this work we establish two fundamental features of Poisson renewal in continuous time. First, we show that renewal dynamics formulated in continuous time can naturally give rise to a mixed discrete–continuous spatial structure. Second, we demonstrate that in an ensemble of particles under renewal, collective effects can induce persistent non-stationary behavior even under Poissonian renewal. We focus on stochastic resetting [17], a simple realization of renewal dynamics in which the evolution of a system is intermittently interrupted by events that return it to a prescribed configuration. Resetting has been shown to strongly affect transport, relaxation, and first-passage properties, and has been explored in a wide range of contexts, including stochastic search and foraging, reaction and enzyme kinetics, and population dynamics [18–26]. For a single particle, CTRW under resetting to the initial position has been studied primarily in the diffusion limit [27, 28]. In this regime, reinitialization of the continuous-time clock leads to dynamics that closely resemble Brownian motion with stochastic resetting. Below we show that this picture does not extend to a general continuous-time formulation of renewal resetting even for a single particle, and that collective interactions can fundamentally modify the impact of renewal. In particular, in contrast to the single-particle

case, macroscopic memory can emerge even when all microscopic reset events are memoryless.

Resetting in many-body systems has been studied in a variety of settings, generating rich collective behavior [29–37]. While these studies employ renewal-based descriptions, a systematic treatment of interacting anomalous transport under reset remains challenging. Recently, an age-structured hydrodynamic framework has been proposed to describe the collective dynamics of ensembles of anomalously diffusing particles subject to renewal resets [38]. Here we expand and generalize this approach to derive a description of CTRW particles undergoing collective Poisson resets.

Model definition and main results. We consider an ensemble of N particles performing CTRW on the line. Each particle alternates between waiting periods and jumps, with waiting times τ sampled from a power-law distribution $\psi(\tau)$ and jump displacements ξ sampled from a kernel $\omega(\xi)$. For concreteness, we take

$$\psi(\tau) = \beta \tau_0^{-1} (1 + \tau/\tau_0)^{-1-\beta}, \quad \omega(\xi) = \frac{1}{2\ell} e^{-|\xi|/\ell}, \quad (1)$$

with $\beta > 0$ and survival probability $\Psi(\tau) = (1 + \tau/\tau_0)^{-\beta}$; our main results are independent of these specific choices. Reset events occur at global rate rN : at each reset, selected particles – see different protocols below – are instantaneously returned to the origin $x = 0$ and their renewal clocks are reset by sampling a new waiting time τ from $\psi(\tau)$. The rate rN is chosen so that in the absence of collective effects, each particle resets at rate r .

Our first central finding is that regardless of the reset protocol, a macroscopic fraction of particles occupies a discrete state at the reset location – a hallmark we attribute to renewal dynamics. This discrete state is generic, does not depend on the specific forms of $\psi(\tau)$ and $\omega(\xi)$, and vanishes only in the diffusion limit.

Next, we establish that collective effects can generate long-term memory. We contrast two reset protocols: independent resets, where particles are randomly selected for reset, and extremal resets, where the particle farthest

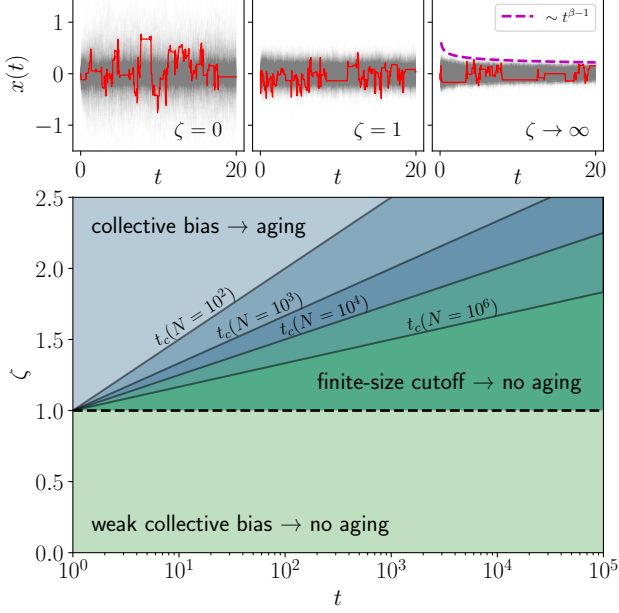


FIG. 1. **Collective renewal and aging.** Top: Simulation trajectory (1 in red overlaid on 10^3 in gray) for reset protocols with different bias exponent ζ . For $\zeta = 0$, independent renewal suppresses aging; for $\zeta = 1$, finite N inhibits collective aging; and for strong bias $\zeta \gg 1$, resets are dominated by extreme particles, leading to nonstationary system size (dashed line) and collective memory ($\beta = 0.8$). Bottom: Dynamical regime diagram in the (t, ζ) plane. For $\zeta > 1$, collective bias induces aging up to a finite-size crossover time $t_c \sim N^{\zeta-1}$.

from the origin is reset. Using the age-structure framework, we show that independent resets lead to a stationary state and reduce the ensemble dynamics to those of a single particle ($N = 1$). By contrast, extremal resets yield a time-dependent solution and persistent aging at long times [39]. The extremal reset rule couples otherwise independent renewal processes through a slowly evolving geometric constraint, generating collective memory.

We further demonstrate that the transition to *collective aging* is discontinuous. To this end, we introduce a reset protocol with collective bias, controlled by exponent ζ that tunes the strength of correlations between particle resets (see definition below), interpolating between independent resets at $\zeta = 0$ and extremal resets at $\zeta \rightarrow \infty$, see Fig. 1. In the limit $N \rightarrow \infty$, the dynamics exhibit a first-order dynamical phase transition at $\zeta = 1$, defined as a non-analytic change in the asymptotic long-time dynamics as the control parameter ζ is varied [40–42]. The transition separates a stationary phase ($\zeta < 1$) from a non-stationary aging phase ($\zeta \geq 1$). At finite N , aging is ultimately cut off, with a crossover time $t_c \sim N^{\zeta-1}$. The resulting dynamical regimes are summarized in Fig. 1.

Independent resets. For independent resets each particle is reset at a constant Poisson rate r , irrespective of the positions of other particles (Fig. 1, $\zeta = 0$). For

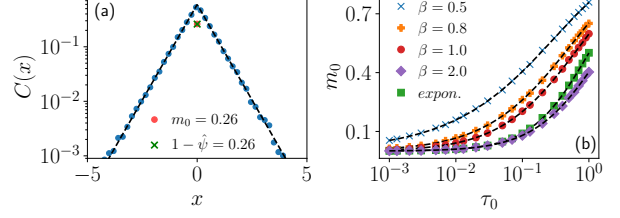


FIG. 2. **Mixed discrete-continuous steady state.** (a) Simulations for the continuous density and delta-peak weight m_0 (blue dots and red dot, respectively) compared to Eq. (3) (dashed line and green x) for $\beta = 0.8$, $\tau_0 = 0.1$. (b) Discrete weight m versus τ_0 for power-law [Eq. (1)] and exponential waiting times. Simulations (see legend), compared to Eq. (3) (dashed line). In both panels, $\tau_0 = \ell^2$, $N = 10^4$, and $t = 10^3$.

$N = 1$ this model was studied in [27, 28]. We describe the collective dynamics using an age-structured theory. Denoting $n(x, \tau, t)$ as the particle density at position x , time t and age τ , we have

$$\partial_t n(x, \tau, t) + \partial_\tau n(x, \tau, t) = -[\beta(\tau) + r] n(x, \tau, t), \quad \tau > 0, \quad (2a)$$

where $\beta(\tau) = \psi(\tau)/\Psi(\tau) = \beta/(\tau_0 + \tau)$. The two loss terms describe renewals due to jumps, which reset the age [43], and independent Poissonian resetting [38]. The boundary condition at $\tau = 0$ collects both contributions,

$$n(x, 0, t) = \int_{\mathbb{R}} dx' \int_0^\infty d\tau' \beta(\tau') \omega(x - x') n(x', \tau', t) + r \delta(x). \quad (2b)$$

The spatial density is $C(x, t) = \int_0^\infty n(x, \tau, t) d\tau$, normalized as $\int_{\mathbb{R}} C(x, t) dx = 1$.

For $t \gg 1$ we seek a steady-state $n_s(x, \tau)$. Setting $\partial_t n = 0$ in Eq. (2a) yields $n(x, \tau) = n(x, 0) \Psi(\tau) e^{-r\tau}$. Introducing the reset-modified survival integral $\tilde{\mu} = \int_0^\infty \Psi(\tau) e^{-r\tau} d\tau$, and $C(x) \equiv C(x, t \gg 1)$, the steady-state solution can be written as $n(x, \tau) = C(x) \Psi(\tau) e^{-r\tau}/\tilde{\mu}$. The factor $e^{-r\tau}$ in $\tilde{\mu}$ implies that resets effectively truncates the heavy-tailed waiting times, rendering $\tilde{\mu}$ finite for all $\beta > 0$. Substituting $n(x, \tau)$ into Eq. (2b) and using $C(x) = \int_0^\infty n(x, \tau) d\tau$, gives a linear inhomogeneous Fredholm integral equation of the second kind,

$$C(x) = \hat{\psi} \int_{\mathbb{R}} \omega(x - x') C(x') dx' + \tilde{\mu} r \delta(x), \quad (3)$$

where $\hat{\psi} = \int_0^\infty \psi(\tau) e^{-r\tau} d\tau$. Noting that $\omega(x)$ is the Green's function of the operator $1 - \ell^2 \partial_x^2$, we apply this operator to Eq. (3) and solve for $C(x)$. This yields,

$$C(x) = [1 - \hat{\psi}] \delta(x) + \frac{\hat{\psi} \sqrt{1 - \hat{\psi}}}{2\ell} e^{-|x| \sqrt{1 - \hat{\psi}}/\ell}. \quad (4)$$

As $\tilde{\mu}$ is finite, a steady-state exists for any $\beta > 0$. Defining m_0 as the delta-peak contribution to the density, Eq. (4) predicts $m_0 = 1 - \hat{\psi}$. In Fig. 2 we compare Eq. (4)

with monte carlo simulations, showing that it holds for both power-law [Eq. (1)] and exponential waiting-times $\psi(\tau) = \tau_0^{-1} e^{-\tau/\tau_0}$ [44]. In the diffusion limit $\ell \rightarrow 0$ with $D_{\text{eff}} \equiv \ell^2/\tilde{\mu}$ fixed, the regular part of $C(x)$ reduces to $C(x) \simeq (1/2)\sqrt{r/D_{\text{eff}}} e^{-|x|\sqrt{r/D_{\text{eff}}}}$, while the delta peak vanishes. This coincides with the result for a single CTRW particle under renewal resets [27, 28].

Our first main result is the emergence of a macroscopic delta peak in Eq. (4), corresponding to particles that have been reset but have not yet jumped. This reflects the generic coexistence of discrete and continuous components in renewal dynamics. Delta-peak contributions are known in aging renewal processes [12], in non-renewal resets [27], and in resets with a refractory period [45]. Here we show that it is an intrinsic consequence of the continuous-time structure and arises independently of the waiting-time law or the resetting protocol (see below), disappearing only in the diffusion limit (Fig. 2b).

Extremal resets. We next consider extremal resets, where at each reset event the particle farthest from the origin is moved to $x = 0$ (Fig. 1, $\zeta \rightarrow \infty$). This protocol was studied for Brownian and scaled Brownian particles [35, 38]. The age-structured equation now reads,

$$\partial_t n(x, \tau, t) + \partial_\tau n(x, \tau, t) = -\beta(\tau) n(x, \tau, t), \quad (5a)$$

for compact support $|x| < L(t)$, with $n(\pm L(t), \tau, t) = 0$ [35]. Unlike independent resets, there is no bulk reset term as resets act only through the boundary. The boundary condition at $\tau = 0$ collects contributions from jumps and resets within the compact support $[-L(t), L(t)]$,

$$n(x, 0, t) = \int_{-L(t)}^{L(t)} dx' \int_0^\infty d\tau' \beta(\tau') \omega(x - x') n(x', \tau', t) + r\delta(x). \quad (5b)$$

The density is $C(x, t) = \int_0^\infty n(x, \tau, t) d\tau$, and the support size is fixed by mass conservation, $\int_{-L(t)}^{L(t)} C(x, t) dx = 1$.

Steady state. For $\beta > 1$, the mean waiting time $\mu = \int_0^\infty \Psi(\tau) d\tau = \tau_0/(\beta - 1)$ is finite, and we derive an integral equation for the steady-state density [44]:

$$C(x) = \frac{1}{2\ell} \int_{-L}^L e^{-|x-x'|/\ell} C(x') dx' + \mu r\delta(x), \quad |x| < L, \quad (6)$$

with $\int_{-L}^L C(x) dx = 1$. Equation (6) is solved by [44],

$$C(x) = \frac{\mu r}{2\ell^2} (\ell + L - |x|) + \mu r\delta(x), \quad |x| < L, \quad (7)$$

i.e., a compact triangular profile, with a macroscopic delta peak $m_0 = \mu r$ at $x = 0$, and discontinuous at the boundaries $\pm L$. The support L follows from normalization, $L = \ell(-1 + \sqrt{2/(\mu r) - 1})$. Comparison with simulations is shown in Fig. 3(a). In the diffusion limit $\ell \ll L$ with $D_{\text{eff}} = \ell^2/\mu$ fixed, Eq. (7) reduces to

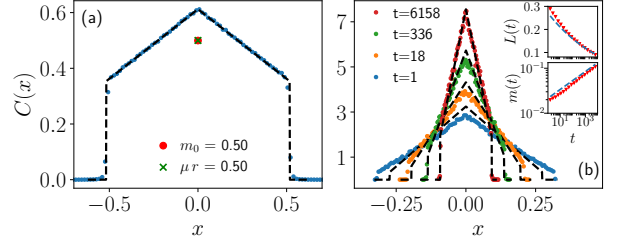


FIG. 3. **Extremal resets.** (a) Steady state. Simulations for the continuous density and delta-peak weight (blue dots and red dot, respectively) compared to Eq. (7) (dashed line, green x) for $\beta = 2$ and $\tau_0 = \ell^2 = 0.5$. (b) Nonstationary regime. Simulations at different t (legend) compared to Eq. (10) (dashed lines). Insets: system size $L(t)$ and condensation $m(t)$, Eq. (11) (dashed lines) compared to simulations (triangles), for $\beta = 0.8$ and $\tau_0 = \ell^2 = 0.001$. In both panels $N = 10^5$ and $r = 1$.

$C(x) \simeq r/(2D_{\text{eff}}) (L - |x|)$, with $L \simeq \sqrt{2D_{\text{eff}}/r}$, in agreement with [35].

Time-dependent solution and aging. For $\beta < 1$ and extremal resets, no steady state exists, and equation (5a) can be solved along characteristics, $n(x, \tau, t) = n(x, 0, t - \tau) \Psi(\tau)$, leading to the exact evolution equation [44],

$$\partial_t C(x, t) = \int_{-L(t)}^{L(t)} \omega(x - x') J(x', t) dx' - J(x, t) + r\delta(x), \quad (8)$$

where the jump flux $J(x, t)$ is given by the convolution $J(x, t) = \int_0^t \Phi(t - \tau) C(x, \tau) d\tau$, and the memory kernel $\Phi(t)$ is defined via its Laplace transform $\hat{\Phi}(s) = s\hat{\psi}(s)/[1 - \hat{\psi}(s)]$. We seek a solution to Eq. (8) in the limit $t \gg 1$, corresponding to $s \ll 1$ [14]. For $\psi(\tau)$ with $\beta < 1$, we have $1 - \hat{\psi}(s) \simeq \Gamma(1 - \beta)(\tau_0 s)^\beta$, implying an algebraically decaying memory kernel $\Phi(t) \simeq (1 - \beta) \sin(\pi\beta) \pi^{-1} \tau_0^{-\beta} t^{\beta-2}$ for $t \rightarrow \infty$. This slow decay reflects the aging of the underlying renewal process and induces non-stationary evolution of $C(x, t)$. In the diffusion limit, Eq. (8) reduces to a fractional Fokker-Planck equation on a compact support [44], consistent with similar long-time limits [14, 46].

For long times, we apply an adiabatic approximation [44]. For $t \gg 1$, the density $C(x, t)$ varies slowly compared to the memory kernel, allowing the closure $J(x, t) \simeq C(x, t) \lambda(t)$, with renewal rate,

$$\lambda(t) \equiv \int_0^t \Phi(t - \tau) d\tau \simeq \frac{\sin(\pi\beta)}{\pi \tau_0^\beta} t^{\beta-1}. \quad (9)$$

Using (9), Eq. (8) reduces to a quasi-static equation identical in form to Eq. (6) for $\beta > 1$, with the replacement $\mu r \rightarrow r/\lambda(t)$ [44]. It then follows that,

$$C(x, t) \simeq \frac{r}{2\ell^2 \lambda(t)} (\ell + L(t) - |x|) + \frac{r}{\lambda(t)} \delta(x), \quad |x| < L(t), \quad (10)$$

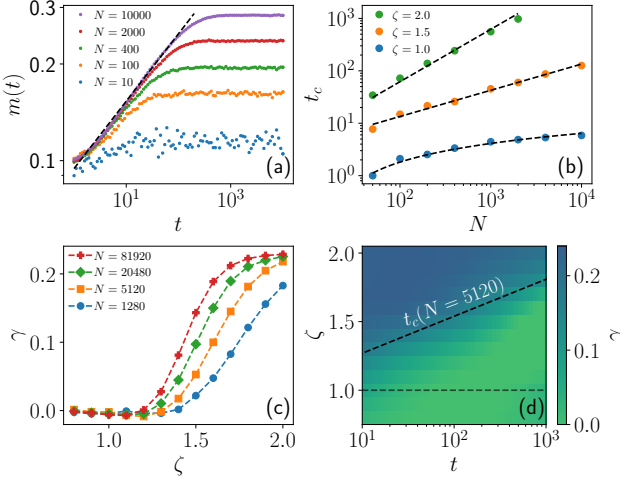


FIG. 4. **Dynamical phase transition induced by collective bias.** (a) Discrete weight $m(t)$ for different N (see legend) and $\zeta = 1.5$, showing an aging regime followed by saturation due to finite-size effects. Compared to the theoretical prediction $m(t) \sim t^{1-\beta}$ (dashed line). (b) Finite-size cutoff time t_c versus N for different ζ (see legend), with the scalings $t_c \sim \log N$ at $\zeta = 1$ and $t_c \sim N^{\zeta-1}$ for $\zeta > 1$ (dashed lines). (c) Aging exponent $\gamma \equiv d \log C(0, t) / d \log t$ as a function of ζ , for different N at $t = 10^2$. (d) Map of γ versus ζ and t (see colorbar) for $N = 5120$. Dashed lines denote $\zeta = 1$ and the theoretical $t_c \sim N^{\zeta-1}$. In all panels, $\beta = 0.8$, $\tau_0 = \ell^2 = 0.01$, and $r = 1$.

and normalization fixes $L(t) \simeq \ell(\sqrt{2\lambda(t)/r - 1} - 1)$. Using Eq. (9), the second main result of this manuscript is the slow decay of the system size $L(t)$ and the slowly increasing condensation at the delta-peak $m(t)$,

$$L(t) \propto t^{(\beta-1)/2}, \quad m(t) = r/\lambda(t) \propto t^{1-\beta}. \quad (11)$$

Defining $\gamma = d \log C(0, t) / d \log t$ we have $\gamma = 1 - \beta$. In Fig. 3(b) we compare Eqs. (10-11) to simulations. An eventual collapse of the support occurs for $\lambda(t_*) = r$, leading to a collapse time $t_* \sim \tau_0^{-\beta/(1-\beta)}$ [44].

Collective bias resets. To investigate the onset of collective aging, we introduce a family of collective reset protocols based on particle rank, which interpolate between independent and extremal resets. At each reset, particles are ranked by their distance from the origin, with rank $k = 1$ ($k = N$) denoting the particle with the largest (smallest) $|x|$, and the probability to reset a particle decreases as $k^{-\zeta}$, so that particles farther from the origin are preferentially reset. For $\zeta = 0$, all ranks are equally likely and resets are independent, while increasing ζ progressively concentrates reset events onto extreme particles, with $\zeta \rightarrow \infty$ recovering extremal resets [44].

Within the age-structured framework, the governing equations take the same form as Eqs. (2), with the constant reset rate r in Eq. (2a) replaced by an effective rate $\alpha(x, t)$ that depends explicitly on the density $C(x, t)$, due to collective bias. While the resulting equations are nonlinear and nonlocal in time – see [44] and Fig. S1,

for a more detailed analysis – we focus here on the spatial structure of $\alpha(x, t)$ at long times $t \gg 1$. In [44], we show that the effective rate $\alpha(x, t)$ induces an effective exponential cutoff of the waiting-time distribution, $\Psi_{\text{eff}}(\tau|x, t) = \Psi(\tau) e^{-\alpha(x, t)\tau}$, such that the asymptotic value of α in the bulk controls whether long waiting times are truncated, see discussion above Eq. (3). Specifically, we find that in the bulk $\alpha_{\text{bulk}} = O(1)$ for $\zeta < 1$, while for $\zeta > 1$ it scales as $\alpha_{\text{bulk}} = O(N^{1-\zeta})$, and at the singular value $\zeta = 1$ one has $\alpha_{\text{bulk}} = O(1/\log N)$. Thus, in the limit $N \rightarrow \infty$, $\alpha_{\text{bulk}} \rightarrow 0$ for all $\zeta \geq 1$, and reset events become asymptotically ineffective in the bulk while remaining strong in the tail, where extreme particles dominate the reset statistics. Focusing on the regime $\beta < 1$, this underlies a first-order dynamical transition at $\zeta = 1$: vanishing α_{bulk} for all $\zeta \geq 1$ implies that resets fail to truncate long waiting times in the bulk, the renewal rate decays algebraically, and the dynamics become nonstationary and exhibit aging [44]. Consequently, the aging exponent γ jumps discontinuously from 0 to $1-\beta$ at $\zeta = 1$.

For any finite N , however, α_{bulk} remains nonzero, yielding a finite cutoff time $t_c \sim 1/\alpha_{\text{bulk}}$, beyond which stationarity is eventually restored. Specifically, at the critical point $\zeta = 1$ one finds $t_c \sim \log N$, while for $\zeta > 1$ the cutoff time scales algebraically as $t_c \sim N^{\zeta-1}$ [44]. Figure 4 summarizes these results for $\beta = 0.8$, illustrating aging of the condensation $m(t)$ for $1 \ll t < t_c$ [4(a)] and the scaling of a finite-size cutoff time t_c with N [4(b)]. We further show that at fixed time, the dynamical transition sharpens and approaches $\zeta = 1$ as N increases [4(c)]. Finally, for $\zeta < 1$ or $t > t_c$ the dynamics are stationary with $\gamma \simeq 0$, while for $\zeta > 1$ and $t < t_c$ we have a sharp transition to aging with $\gamma \simeq 1 - \beta$ [4(d)].

Discussion. As an illustrative ecological example, CTRW provide a consistent description of breeding white storks movement [9, 10]. Storks perform ~ 3 daily foraging bouts with patch residence times of 30–70 min and inter-site distances of 200–400 m [47], corresponding to $\tau_0 \in [0.5, 1.2]$ h, $\ell \in [0.2, 0.4]$ km, and $r \sim 3$ day $^{-1}$. These values are far from the diffusion limit (see above), and are therefore consistent with our mixed discrete–continuous spatial structure, including condensation at the nest and potentially other repeatedly visited locations [48]. Furthermore, foraging behavior in this species is strongly shaped by collective decision-making [49, 50]. While the collective-bias models are highly simplified, our framework provides a general method for probing how collective bias qualitatively modifies long-time statistics.

Although we focus on resetting, our results show that interactions in continuous time dynamics can fundamentally alter memoryless renewal processes, allowing non-Markovian effects to emerge. These results are relevant to other renewal processes, including population dynamics with prolonged sojourns at local extinction [51], neuronal spiking models with refractory renewal statistics [52], and learning processes driven by restarts [53].

Acknowledgment. We are grateful to Baruch Meerson, Eli Barkai, and Naftali Smith for invaluable discussions.

* ohad.vilk@mail.huji.ac.il

[1] X. Brokmann, J.-P. Hermier, G. Messin, P. Desbiolles, J.-P. Bouchaud, and M. Dahan, Statistical aging and nonergodicity in the fluorescence of single nanocrystals, *Phys. Rev. Lett.* **90**, 120601 (2003).

[2] S. Bianco, M. Ignaccolo, M. S. Rider, M. J. Ross, P. Winsor, and P. Grigolini, Brain, music, and non-poisson renewal processes, *Phys. Rev. E* **75**, 061911 (2007).

[3] M. C. Gonzalez, C. A. Hidalgo, and A.-L. Barabasi, Understanding individual human mobility patterns, *Nature* **453**, 779 (2008).

[4] V. Zaburdaev, S. Denisov, and J. Klafter, Lévy walks, *Rev. Mod. Phys.* **87**, 483 (2015).

[5] J.-H. Jeon, V. Tejedor, S. Burov, E. Barkai, C. Selhuber-Unkel, K. Berg-Sørensen, L. Oddershede, and R. Metzler, In vivo anomalous diffusion and weak ergodicity breaking of lipid granules, *Phys. Rev. Lett.* **106**, 048103 (2011).

[6] A. V. Weigel, B. Simon, M. M. Tamkun, and D. Krapf, Ergodic and nonergodic processes coexist in the plasma membrane as observed by single-molecule tracking, *PNAS* **108**, 6438 (2011).

[7] E. Barkai and S. Burov, Packets of diffusing particles exhibit universal exponential tails, *Phys. Rev. Lett.* **124**, 060603 (2020).

[8] O. Vilk, Y. Orchan, M. Charter, N. Ganot, S. Toledo, R. Nathan, and M. Assaf, Ergodicity breaking in area-restricted search of avian predators, *Phys. Rev. X* **12**, 031005 (2022).

[9] O. Vilk, E. Aghion, T. Avgar, C. Beta, O. Nagel, A. Sabri, R. Sarfati, D. K. Schwartz, M. Weiss, D. Krapf, *et al.*, Unravelling the origins of anomalous diffusion: From molecules to migrating storks, *Phys. Rev. Res.* **4**, 033055 (2022).

[10] O. Vilk, E. Aghion, R. Nathan, S. Toledo, R. Metzler, and M. Assaf, Classification of anomalous diffusion in animal movement data using power spectral analysis, *J. Phys. A: Math. Theor.* **55**, 334004 (2022).

[11] C. Godreche and J. Luck, Statistics of the occupation time of renewal processes, *J. Stat. Phys.* **104**, 489 (2001).

[12] J. H. Schulz, E. Barkai, and R. Metzler, Aging renewal theory and application to random walks, *Phys. Rev. X* **4**, 011028 (2014).

[13] R. Cakir, P. Grigolini, and A. A. Krokhin, Dynamical origin of memory and renewal, *Phys. Rev. E—Statistical, Nonlinear, and Soft Matter Physics* **74**, 021108 (2006).

[14] R. Metzler and J. Klafter, The random walk's guide to anomalous diffusion: a fractional dynamics approach, *Phys. Rep.* **339**, 1 (2000).

[15] G. Bel and E. Barkai, Weak ergodicity breaking in the continuous-time random walk, *Phys. Rev. Lett.* **94**, 240602 (2005).

[16] R. Metzler, J.-H. Jeon, A. G. Cherstvy, and E. Barkai, Anomalous diffusion models and their properties: non-stationarity, non-ergodicity, and ageing at the centenary of single particle tracking, *Phys. Chem. Chem. Phys.* **16**, 24128 (2014).

[17] M. R. Evans and S. N. Majumdar, Diffusion with stochastic resetting, *Phys. Rev. Lett.* **106**, 160601 (2011).

[18] S. Reuveni, M. Urbakh, and J. Klafter, The role of substrate unbinding in michaelis-menten enzymatic reactions, *Biophys. J.* **106**, 677a (2014).

[19] A. Kundu and S. Reuveni, Preface: stochastic resetting—theory and applications, *J. Phys. A: Math. Theor.* **57**, 060301 (2024).

[20] J. R. Koenig, O. Padon, and A. Aiken, Adaptive restarts for stochastic synthesis, in *Proceedings of the 42nd ACM SIGPLAN International Conference on Programming Language Design and Implementation* (2021) pp. 696–709.

[21] S. Picardi, B. J. Smith, M. E. Boone, P. C. Frederick, J. G. Cecere, D. Rubolini, L. Serra, S. Pirrello, R. R. Borkhataria, and M. Basille, Analysis of movement recursions to detect reproductive events and estimate their fate in central place foragers, *Mov. Ecol.* **8**, 24 (2020).

[22] O. Blumer, S. Reuveni, and B. Hirshberg, Stochastic resetting for enhanced sampling, *J. Phys. Chem. Lett.* **13**, 11230 (2022).

[23] M. R. Evans, S. N. Majumdar, and G. Schehr, Stochastic resetting and applications, *J. Phys. A: Math. Theor.* **53**, 193001 (2020).

[24] S. Gupta and A. M. Jayannavar, Stochastic resetting: A (very) brief review, *Front. Phys.* **10**, 789097 (2022).

[25] S. Meir, T. D. Keidar, S. Reuveni, and B. Hirshberg, First-passage approach to optimizing perturbations for improved training of machine learning models, *MLST* **6**, 025053 (2025).

[26] J. R. Church, O. Blumer, T. D. Keidar, L. Ploutno, S. Reuveni, and B. Hirshberg, Accelerating molecular dynamics through informed resetting, *J. Chem. Theory Comput.* **21**, 605 (2025).

[27] Ł. Kuśmierz and E. Gudowska-Nowak, Subdiffusive continuous-time random walks with stochastic resetting, *Phys. Rev. E* **99**, 052116 (2019).

[28] A. Masó-Puigdellosas, D. Campos, and V. Méndez, Transport properties and first-arrival statistics of random motion with stochastic reset times, *Phys. Rev. E* **99**, 012141 (2019).

[29] A. Nagar and S. Gupta, Stochastic resetting in interacting particle systems: A review, *J. Phys. A: Math. Theor.* **56**, 283001 (2023).

[30] M. Siboni, P. Sasorov, and B. Meerson, Fluctuations of a swarm of Brownian bees, *Phys. Rev. E* **104**, 054131 (2021).

[31] R. Vatash and Y. Roichman, Many-body colloidal dynamics under stochastic resetting: Competing effects of particle interactions on the steady-state distribution, *Phys. Rev. Res.* **7**, L032020 (2025).

[32] M. Biroli, H. Larralde, S. N. Majumdar, and G. Schehr, Extreme statistics and spacing distribution in a Brownian gas correlated by resetting, *Phys. Rev. Lett.* **130**, 207101 (2023).

[33] M. Biroli, S. N. Majumdar, and G. Schehr, Resetting dyson Brownian motion, *Phys. Rev. E* **112**, 014101 (2025).

[34] O. Vilk and B. Meerson, Collective behavior of independent scaled Brownian particles with renewal resetting, *arXiv preprint arXiv:2512.21061* (2025).

[35] O. Vilk, M. Assaf, and B. Meerson, Fluctuations and first-passage properties of systems of Brownian particles with reset, *Phys. Rev. E* **106**, 024117 (2022).

[36] J. Berestycki, É. Brunet, J. Nolen, and S. Penington, Brownian bees in the infinite swarm limit, *Ann. Probab.* **50**, 2133 (2022).

[37] J. Berestycki, É. Brunet, J. Nolen, and S. Penington, A free boundary problem arising from branching Brownian motion with selection, *Trans. Am. Math. Soc.* **374**, 6269 (2021).

[38] B. Meerson and O. Vilk, Age-structured hydrodynamics of ensembles of anomalously diffusing particles with renewal resetting, *arXiv:2512.1434* (2025).

[39] Aging is defined here as the breakdown of time-translation invariance in macroscopic observables, manifested by their explicit dependence on the time since system preparation. In renewal processes, this is typically associated with a time-dependent renewal rate.

[40] J. P. Garrahan, R. L. Jack, V. Lecomte, E. Pitard, K. van Duijvendijk, and F. van Wijland, Dynamical first-order phase transition in kinetically constrained models of glasses, *Phys. Rev. Lett.* **98**, 195702 (2007).

[41] G. Gradenigo and S. N. Majumdar, A first-order dynamical transition in the displacement distribution of a driven run-and-tumble particle, *J. Stat. Mech. Theory Exp.* **2019**, 053206 (2019).

[42] J. Meibohm and M. Esposito, Finite-time dynamical phase transition in nonequilibrium relaxation, *Phys. Rev. Lett.* **128**, 110603 (2022).

[43] H. Berry, T. Lepoutre, and Á. M. González, Quantitative convergence towards a self-similar profile in an age-structured renewal equation for subdiffusion, *Acta Appl. Math.* **145**, 15 (2016).

[44] See supplemental information at [url] for complete derivations, additional results from our analysis, and details on the Monte Carlo simulations.

[45] M. R. Evans and S. N. Majumdar, Effects of refractory period on stochastic resetting, *J. Phys. A: Math. Theor.* **52**, 01LT01 (2018).

[46] M. M. Meerschaert and H.-P. Scheffler, Limit theorems for continuous-time random walks with infinite mean waiting times, *J. Appl. Probab.* **41**, 623 (2004).

[47] J. C. Alonso, J. A. Alonso, and L. M. Carrascal, Habitat selection by foraging white storks, *ciconia ciconia*, during the breeding season, *Canadian Journal of Zoology* **69**, 1957 (1991).

[48] D. Zurell, H. Von Wehrden, S. Rotics, M. Kaatz, H. Groß, L. Schlag, M. Schäfer, N. Sapir, S. Turjeman, M. Wikelski, *et al.*, Home range size and resource use of breeding and non-breeding white storks along a land use gradient, *Front. Ecol. Evol.* **6**, 79 (2018).

[49] G. Blanco, Population dynamics and communal roosting of white storks foraging at a spanish refuse dump, *Colonial Waterbirds* , 273 (1996).

[50] A. Flack, M. Nagy, W. Fiedler, I. D. Couzin, and M. Wikelski, From local collective behavior to global migratory patterns in white storks, *Science* **360**, 911 (2018).

[51] R. Lande, S. Engen, and B.-E. Sæther, Extinction times in finite metapopulation models with stochastic local dynamics, *Oikos* , 383 (1998).

[52] A. N. Burkitt, A review of the integrate-and-fire neuron model: I. homogeneous synaptic input, *Biological cybernetics* **95**, 1 (2006).

[53] H. Kautz, E. Horvitz, Y. Ruan, C. Gomes, and B. Selman, Dynamic restart policies, *Aaaai/iaai* **97**, 674 (2002).

**SUPPLEMENTARY INFORMATION FOR MACROSCOPIC LOCALIZATION AND COLLECTIVE
MEMORY IN POISSON RENEWAL RESETTING**

In this supplementary information we provide Sec. S1-S4, and Fig. S1 to support the derivations in the main text. In what follows, the notations and abbreviations are the same as in the main text and the equations and figures refer to those therein.

CONTENTS

References	5
Supplementary Information for Macroscopic localization and collective memory in Poisson renewal resetting	7
S1: Independent resetting	8
Power-law waiting times	8
Exponential waiting times	8
S2: Extremal resetting	9
Age-structured equations	9
Stationary solution for $\beta > 1$	9
Time-dependent solution for $\beta < 1$	11
Long-time asymptotics	11
Fractional Fokker-Planck form	12
Adiabatic approximation	13
S3: Rank-based resetting	14
Age-structured equations	14
Reduction to independent resetting ($\zeta = 0$)	14
Reduction to extremal resetting ($\zeta \rightarrow \infty$)	15
Steady state for $\beta > 1$	15
Large- $ x $ behavior (tail)	16
Bulk behavior	17
Time-dependent regime for $\beta < 1$	19
S4: Monte Carlo simulations	20

S1: INDEPENDENT RESETTING

In the main text we derived the stationary spatial density for independent Poissonian resetting [Eq. (4)],

$$C(x) = [1 - \hat{\psi}] \delta(x) + \frac{\hat{\psi} \sqrt{1 - \hat{\psi}}}{2\ell} \exp\left(-\frac{|x|}{\ell} \sqrt{1 - \hat{\psi}}\right), \quad (\text{S1})$$

where $\hat{\psi} \equiv \int_0^\infty \psi(\tau) e^{-r\tau} d\tau$, and ℓ is the characteristic jump length of the exponential kernel $\omega(\xi) = (2\ell)^{-1} e^{-|\xi|/\ell}$. Here we give explicit expressions for $\hat{\psi}$ and $C(x)$ for power-law and exponential waiting-time distributions – as used in Fig. 2 of the main text.

Power-law waiting times

For the waiting-time in Eq. (1) of the main text $\hat{\psi}$ is given by

$$\hat{\psi} = \int_0^\infty \psi(\tau) e^{-r\tau} d\tau = \beta e^{r\tau_0} E_{\beta+1}(r\tau_0), \quad (\text{S2})$$

where $E_\nu(z) = \int_1^\infty e^{-zu} u^{-\nu} du$ is the exponential integral. Substituting Eq. (S2) into Eq. (S1) yields the stationary density

$$C(x) = \left[1 - \beta e^{r\tau_0} E_{\beta+1}(r\tau_0)\right] \delta(x) + \frac{\beta e^{r\tau_0} E_{\beta+1}(r\tau_0) \sqrt{1 - \beta e^{r\tau_0} E_{\beta+1}(r\tau_0)}}{2\ell} e^{-\frac{|x|}{\ell} \sqrt{1 - \beta e^{r\tau_0} E_{\beta+1}(r\tau_0)}}. \quad (\text{S3})$$

Exponential waiting times

For Poissonian waiting times with mean τ_0 ,

$$\psi(\tau) = \frac{1}{\tau_0} e^{-\tau/\tau_0}, \quad (\text{S4})$$

$\hat{\psi}$ is given by

$$\hat{\psi} = \frac{1}{1 + r\tau_0}. \quad (\text{S5})$$

Equation (S1) then gives the explicit stationary density

$$C(x) = \frac{r\tau_0}{1 + r\tau_0} \delta(x) + \frac{1}{2\ell \sqrt{r\tau_0(1 + r\tau_0)}} \exp\left(-\frac{|x|}{\ell} \sqrt{\frac{r\tau_0}{1 + r\tau_0}}\right). \quad (\text{S6})$$

S2: EXTREMAL RESETTING

Here we provide a detailed derivation for the extremal resetting protocol.

Age-structured equations

As detailed in the main text, the age τ denotes the time elapsed since the last jump or reset. We denote by $n(x, \tau, t)$ the age-structured particle density and by $C(x, t) = \int_0^\infty n(x, \tau, t) d\tau$, the corresponding spatial density. Due to extremal resetting, particles are confined to a compact support $|x| < L(t)$ [35]. Inside the support $|x| < L(t)$ and away from $\tau = 0$, the age-structured density satisfies [Eq. (5a) in the main text]

$$\partial_t n(x, \tau, t) + \partial_\tau n(x, \tau, t) = -\beta(\tau) n(x, \tau, t), \quad |x| < L(t), \quad \tau > 0. \quad (\text{S7})$$

In contrast to independent resetting, there is no bulk resetting loss term: reset events act only on the most extreme particle and therefore affect the dynamics solely through the moving boundary $L(t)$. Age renewal ($\tau \rightarrow 0$) occurs both due to CTRW jumps and due to extremal reset events. The boundary condition at $\tau = 0$ is therefore given by [Eq. (5b) in the main text]

$$n(x, 0, t) = \int_{-L(t)}^{L(t)} dx' \int_0^\infty d\tau' \beta(\tau') \omega(x - x') n(x', \tau', t) + r \delta(x), \quad (\text{S8})$$

where the first term accounts for renewal after jumps and the second term describes reinjection at the origin following extremal resets. The size of the support $L(t)$ is determined self-consistently by mass conservation,

$$\int_{-L(t)}^{L(t)} C(x, t) dx = 1, \quad (\text{S9})$$

ensuring that the total number of particles is conserved at all times.

Stationary solution for $\beta > 1$

For $\beta > 1$ the mean waiting time

$$\mu = \int_0^\infty \Psi(\tau) d\tau$$

is finite, and a stationary solution may exist. Assuming $\partial_t n_s = 0$, Eq. (S7) reduces to an ordinary differential equation in the age variable,

$$\partial_\tau n_s(x, \tau) = -\frac{\beta}{\tau_0 + \tau} n_s(x, \tau), \quad (\text{S10})$$

whose solution is

$$n_s(x, \tau) = C(x) \frac{\Psi(\tau)}{\mu}, \quad \mu = \int_0^\infty \Psi(\tau) d\tau = \frac{\tau_0}{\beta - 1}. \quad (\text{S11})$$

Substituting Eq. (S11) into the boundary condition (S8) yields a closed equation for the stationary spatial density,

$$C(x) = \frac{1}{2\ell} \int_{-L}^L e^{-|x-x'|/\ell} C(x') dx' + \mu r \delta(x), \quad |x| < L, \quad (\text{S12})$$

together with the normalization condition

$$\int_{-L}^L C(x) dx = 1, \quad (\text{S13})$$

where the support size L is to be determined. Equation (S12) corresponds to Eq. (6) in the main text. To solve Eq. (S12), we introduce the integral operator

$$(Kf)(x) := \int_{-L}^L \omega(x - x') f(x') dx', \quad \omega(x) = \frac{1}{2\ell} e^{-|x|/\ell}.$$

For any integrable function f , the function $u(x) := (Kf)(x)$ satisfies one-sided endpoint relations. Indeed, for $x \rightarrow L^-$ one has $|x - x'| = x - x'$ for all $x' \in [-L, L]$, so that

$$u(x) = \frac{e^{-x/\ell}}{2\ell} \int_{-L}^L e^{x'/\ell} f(x') dx', \quad x \lesssim L,$$

and hence

$$u'(L^-) = -\frac{1}{\ell} u(L^-). \quad (\text{S14})$$

Similarly, for $x \rightarrow -L^+$ one finds

$$u'(-L^+) = +\frac{1}{\ell} u(-L^+). \quad (\text{S15})$$

We emphasize that the boundary conditions here are *not* $C(\pm L) = 0$, indicating that the stationary density may be discontinuous at the edges of the support. This contrasts with the Brownian [35] and scaled-Brownian [38] cases, that are only well defined in the diffusion limit where the density is by construction continuous. To proceed, we decompose the density as

$$C(x) = c(x) + \mu r \delta(x),$$

where $c(x)$ is regular on $(-L, L)$. Substituting into Eq. (S12) gives

$$c(x) = (Kc)(x) + \mu r \omega(x), \quad |x| < L. \quad (\text{S16})$$

Let $u := Kc$. Then $c = u + \mu r \omega$. Using the Green's-function identity

$$(1 - \ell^2 \partial_x^2) \omega(x) = \delta(x), \quad (1 - \ell^2 \partial_x^2)(Kf) = f,$$

and applying $(1 - \ell^2 \partial_x^2)$ to $c = u + \mu r \omega$, we obtain

$$-\ell^2 c''(x) = \mu r \delta(x).$$

Thus c is piecewise linear and satisfies the slope jump condition

$$c''(x) = 0 \quad (x \neq 0), \quad c'(0^+) - c'(0^-) = -\frac{\mu r}{\ell^2}. \quad (\text{S17})$$

By symmetry the solution is even, so $c(x) = a - b|x|$ for $|x| < L$. Using Eq. (S17) gives $2b = \mu r / \ell^2$, i.e. $b = \mu r / (2\ell^2)$. The intercept a is fixed using the endpoint condition for $u = Kc = c - \mu r \omega$. Evaluating $u'(L^-) = -(1/\ell)u(L^-)$ and using $\omega'(L) = -(1/\ell)\omega(L)$ yields $a = b(L + \ell)$. Hence

$$c(x) = \frac{\mu r}{2\ell^2} (\ell + L - |x|), \quad |x| < L, \quad (\text{S18})$$

and the full stationary density reads

$$C(x) = \frac{\mu r}{2\ell^2} (\ell + L - |x|) + \mu r \delta(x), \quad |x| < L. \quad (\text{S19})$$

Finally, imposing the normalization condition (S13) gives

$$1 = \int_{-L}^L c(x) dx + \mu r = \mu r \left(1 + \frac{L}{\ell} + \frac{L^2}{2\ell^2} \right). \quad (\text{S20})$$

Solving for L yields

$$L = \ell \left(-1 + \sqrt{\frac{2}{\mu r} - 1} \right) \simeq \sqrt{\frac{2\ell^2}{\mu r}}, \quad (\text{S21})$$

which requires $0 < \mu r \leq 1$ to ensure $L \geq 0$; the final approximation assumes $\mu r \ll 1$. Equation (S19) correspond to Eq. (7) in the main text, and (S21) appears below Eq. (7).

Time-dependent solution for $\beta < 1$

We now consider the regime $\beta < 1$, for which the mean waiting time diverges and no stationary state exists. Our goal is to derive a closed, time-dependent evolution equation for the spatial density $C(x, t)$ starting from the age-structured formulation. The bulk equation (S7) is time dependent and can be solved explicitly along characteristics. For $0 < \tau < t$ one finds

$$n(x, \tau, t) = n(x, 0, t - \tau) \Psi(\tau), \quad (\text{S22})$$

where $\Psi(\tau) = \int_{\tau}^{\infty} \psi(s) ds$ is the survival probability. This representation is exact and holds for all $\beta > 0$. We define the local renewal (jump) flux

$$J(x, t) = \int_0^{\infty} \beta(\tau) n(x, \tau, t) d\tau. \quad (\text{S23})$$

Substituting Eq. (S22) into these definitions yields the Volterra representations

$$C(x, t) = \int_0^t \Psi(\tau) n(x, 0, t - \tau) d\tau + C_{\text{ic}}(x, t), \quad (\text{S24})$$

$$J(x, t) = \int_0^t \psi(\tau) n(x, 0, t - \tau) d\tau + J_{\text{ic}}(x, t), \quad (\text{S25})$$

where C_{ic} and J_{ic} depend on the initial age distribution. For $\beta < 1$ these contributions decay algebraically and become negligible at long times. Integrating Eq. (S7) over $\tau \in (0, \infty)$ and using $n(x, \infty, t) = 0$ yields

$$\partial_t C(x, t) = n(x, 0, t) - J(x, t). \quad (\text{S26})$$

Substituting the boundary condition (S8) into Eq. (S26) gives a closed evolution equation for the spatial density,

$$\partial_t C(x, t) = \int_{-L(t)}^{L(t)} \omega(x - x') J(x', t) dx' - J(x, t) + r \delta(x), \quad |x| < L(t), \quad (\text{S27})$$

where $\omega(\xi)$ is the jump kernel defined in the main text. Equation (S27) is exact and holds for all $\beta > 0$. The Volterra relations (S24)–(S25) can be combined to eliminate $n(x, 0, t)$ and obtain a closed relation between J and C . Taking Laplace transforms in time and neglecting the decaying initial-condition terms yields

$$\hat{J}(x, s) = \hat{\Phi}(s) \hat{C}(x, s), \quad \hat{\Phi}(s) = \frac{s \hat{\psi}(s)}{1 - \hat{\psi}(s)}. \quad (\text{S28})$$

In the time domain this corresponds to the convolution

$$J(x, t) = \int_0^t \Phi(t - \tau) C(x, \tau) d\tau. \quad (\text{S29})$$

Substituting Eq. (S29) into Eq. (S27) yields an exact, nonlocal-in-time integro-differential equation for $C(x, t)$. Equation (S27) thus corresponds to Eq. (8) in the main text.

Long-time asymptotics

We derive the long-time asymptotics for $0 < \beta < 1$. For the waiting-time density $\psi(\tau)$ used in the main text, the Laplace transform has the small- s expansion

$$1 - \hat{\psi}(s) \simeq \Gamma(1 - \beta) (\tau_0 s)^{\beta}, \quad s \rightarrow 0. \quad (\text{S30})$$

Using Eq. (S28), where Φ denotes the memory kernel associated with ψ , this implies

$$\hat{\Phi}(s) \simeq \frac{s^{1-\beta}}{\tau_0^{\beta} \Gamma(1 - \beta)}, \quad s \rightarrow 0. \quad (\text{S31})$$

In the time domain, the corresponding long-time behavior is algebraic,

$$\Phi(t) \simeq \frac{(1-\beta) \sin(\pi\beta)}{\pi \tau_0^\beta} t^{\beta-2}, \quad t \rightarrow \infty. \quad (\text{S32})$$

Substituting Eq. (S32) into Eq. (S29) and then into Eq. (S27) yields the long-time, closed evolution equation

$$\partial_t C(x, t) \simeq \int_{-L(t)}^{L(t)} \omega(x - x') (\Phi * C)(x', t) dx' - (\Phi * C)(x, t) + r \delta(x), \quad (\text{S33})$$

where

$$(\Phi * C)(x, t) = \int_0^t \Phi(t - \tau) C(x, \tau) d\tau.$$

Equation (S33) makes explicit how aging in the renewal process induces slow, non-Markovian dynamics of the spatial density.

Fractional Fokker-Planck form

The long-time tail $\Phi(t) \propto t^{\beta-2}$ implies that the memory term $(\Phi * C)(x, t)$ can be expressed in terms of a fractional time derivative. Indeed, the small- s behavior

$$\hat{\Phi}(s) \sim \frac{1}{\tau_0^\beta \Gamma(1-\beta)} s^{1-\beta} \quad (s \rightarrow 0)$$

corresponds to a fractional derivative of order $1-\beta$. Thus, asymptotically,

$$(\Phi * C)(x, t) \simeq \frac{1}{\tau_0^\beta \Gamma(1-\beta)} D_t^{1-\beta} C(x, t), \quad (\text{S34})$$

where $D_t^{1-\beta}$ may be taken in the Caputo sense (equivalently Riemann–Liouville up to initial data in Laplace space). Substituting Eq. (S34) into Eq. (S33) gives the time-fractional, nonlocal-in-space evolution equation

$$\partial_t C(x, t) \simeq \frac{1}{\tau_0^\beta \Gamma(1-\beta)} \left[\int_{-L(t)}^{L(t)} \omega(x - x') D_t^{1-\beta} C(x', t) dx' - D_t^{1-\beta} C(x, t) \right] + r \delta(x), \quad (\text{S35})$$

valid for $|x| < L(t)$.

In the diffusion limit $\ell \rightarrow 0$ with $D_{\text{eff}} := \ell^2/\tau_0^\beta$ fixed (up to constants), the spatial nonlocality induced by ω reduces to a Laplacian. Although the convolution in Eq. (S35) is truncated to $[-L(t), L(t)]$, the missing contribution is exponentially small for bulk points with $\text{dist}(x, \{\pm L(t)\}) \gg \ell$. Using $\int_{\mathbb{R}} \xi^2 \omega(\xi) d\xi = 2\ell^2$, one obtains the leading-order expansion

$$\int_{-L(t)}^{L(t)} \omega(x - x') f(x', t) dx' - f(x, t) \simeq \ell^2 \partial_x^2 f(x, t), \quad |x| < L(t), \quad (\text{S36})$$

with $f(x, t) = D_t^{1-\beta} C(x, t)$. Substituting into Eq. (S35) yields the local fractional diffusion equation

$$\partial_t C(x, t) \simeq \frac{D_{\text{eff}}}{\Gamma(1-\beta)} D_t^{1-\beta} \partial_x^2 C(x, t) + r \delta(x), \quad |x| < L(t). \quad (\text{S37})$$

The truncation at $\pm L(t)$ produces a boundary layer of width $O(\ell)$; in the sharp diffusion limit this corresponds to an effective Dirichlet condition for the *regular part* of the density at the moving edge,

$$C(\pm L(t), t) = 0, \quad (\text{S38})$$

together with the mass constraint $\int_{-L(t)}^{L(t)} C(x, t) dx = 1$ that determines $L(t)$. Fractional Fokker–Planck/master equations of this type arise as scaling limits of CTRWs with heavy-tailed waiting times; see, e.g., [14, 46] and references therein.

Adiabatic approximation

Returning to Eq. (S33), we derive an adiabatic (quasi-static) approximation for $0 < \beta < 1$. We assume that at long times the spatial density varies slowly over the memory window of the kernel $\Phi(t - \tau)$. Then the renewal flux may be approximated by

$$J(x, t) = \int_0^t \Phi(t - \tau) C(x, \tau) d\tau \simeq C(x, t) \int_0^t \Phi(t - \tau) d\tau = C(x, t) \int_0^t \Phi(u) du \equiv C(x, t) \lambda(t), \quad (\text{S39})$$

where $\lambda(t)$ is the (global) renewal rate associated with the underlying waiting-time law. For the power-law waiting-time density with $0 < \beta < 1$, one has the long-time asymptotic

$$\lambda(t) \simeq \frac{\sin(\pi\beta)}{\pi \tau_0^\beta} t^{\beta-1}, \quad t \rightarrow \infty \quad (\text{S40})$$

which coincides with Eq. (9) of the main text. Substituting Eq. (S39) into Eq. (S27) yields

$$\partial_t C(x, t) \simeq \lambda(t) \left[\int_{-L(t)}^{L(t)} \omega(x - x') C(x', t) dx' - C(x, t) \right] + r \delta(x), \quad |x| < L(t), \quad (\text{S41})$$

valid in the slowly evolving long-time regime. In the adiabatic limit the spatial profile relaxes rapidly compared to the evolution of $\lambda(t)$ and $L(t)$, so we seek a quasi-static solution with $\partial_t C \simeq 0$ at fixed t :

$$C(x, t) \simeq \int_{-L(t)}^{L(t)} \omega(x - x') C(x', t) dx' + \frac{r}{\lambda(t)} \delta(x), \quad |x| < L(t). \quad (\text{S42})$$

This has the same form as the stationary equation (S12) for $\beta > 1$, under the mapping $\mu r \mapsto r/\lambda(t)$. Thus we obtain

$$C(x, t) = \frac{r}{2\ell^2 \lambda(t)} (\ell + L(t) - |x|) + \frac{r}{\lambda(t)} \delta(x), \quad |x| < L(t), \quad (\text{S43})$$

in agreement with Eq. (10) of the main text. Normalization $\int_{-L(t)}^{L(t)} C(x, t) dx = 1$ then gives

$$L(t) = \ell \left(-1 + \sqrt{\frac{2\lambda(t)}{r} - 1} \right) \simeq \ell \sqrt{\frac{2\lambda(t)}{r}}, \quad (\text{S44})$$

where the final approximation assumes $L(t) \gg \ell$ (equivalently $\lambda(t) \gg r$). Using Eq. (S40) yields

$$L(t) \propto t^{(\beta-1)/2}, \quad m(t) \equiv \frac{r}{\lambda(t)} \propto t^{1-\beta}, \quad (\text{S45})$$

which corresponds to Eq. (11) of the main text.

The quasi-static solution (S43) requires $L(t) \geq 0$, which from Eq. (S44) is equivalent to $\lambda(t) \geq r$ (or $m(t) = r/\lambda(t) \leq 1$). Since $\lambda(t) \rightarrow 0$ for $0 < \beta < 1$, the support collapses at a finite time t_* defined by

$$\lambda(t_*) = r. \quad (\text{S46})$$

Using Eq. (S40) gives

$$t_* \sim \left(\frac{\sin(\pi\beta)}{\pi r \tau_0^\beta} \right)^{1/(1-\beta)} \propto \tau_0^{-\beta/(1-\beta)}, \quad (\text{S47})$$

in agreement with the scaling quoted in the main text. The adiabatic approximation is expected to hold for $t \ll t_*$, while it breaks down close to collapse, where $L(t) \rightarrow 0$ and the evolution becomes dominated by the shrinking boundary layer. Notably, in the diffusion limit $t_* \rightarrow \infty$, and there is no finite-time collapse.

Away from collapse, consistency of the adiabatic approximation follows a posteriori from $C(x, t) \sim \lambda(t)^{-1}$, which gives $\partial_t C \sim t^{-\beta} \rightarrow 0$, and from the fact that the kernel $\Phi(t - \tau) \sim (t - \tau)^{\beta-2}$ is dominated by $\tau \approx t$, so that $C(x, \tau)$ varies only weakly over the contributing time window, justifying $(\Phi * C)(x, t) \simeq \lambda(t)C(x, t)$.

S3: RANK-BASED RESETTING

Here we provide a detailed derivation of the rank-based resetting protocol; see the main text for its definition.

Age-structured equations

In the limit $N \gg 1$, rank information is encoded through the tail mass

$$T(s, t) = \int_{|y|>s} C(y, t) dy, \quad (\text{S48})$$

where $C(x, t)$ denotes the one-particle spatial density. The rank-based selection rule is represented by the weight

$$w(x, t) = (1 + N T(|x|, t))^{-\zeta}. \quad (\text{S49})$$

The corresponding normalization factor is

$$Z(t) = \int_{\mathbb{R}} w(x, t) C(x, t) dx. \quad (\text{S50})$$

Let $n(x, \tau, t)$ denote the density of particles at position x and age τ at time t . As in the previous cases, the age-structured evolution equation reads

$$\partial_t n(x, \tau, t) + \partial_{\tau} n(x, \tau, t) = -[\beta(\tau) + \alpha(x, t)] n(x, \tau, t), \quad (\text{S51})$$

where the effective, position-dependent reset rate is

$$\alpha(x, t) = r \frac{w(x, t)}{Z(t)}. \quad (\text{S52})$$

The boundary condition at $\tau = 0$ follows from renewal after jumps and reset-induced injection:

$$n(x, 0, t) = \int_{\mathbb{R}} dx' \int_0^{\infty} d\tau' \beta(\tau') \omega(x - x') n(x', \tau', t) + r \delta(x). \quad (\text{S53})$$

The spatial density is obtained by integrating over ages,

$$C(x, t) = \int_0^{\infty} n(x, \tau, t) d\tau, \quad \int_{\mathbb{R}} C(x, t) dx = 1. \quad (\text{S54})$$

Despite the explicit appearance of N in the microscopic rank-based rule, the above equations are asymptotically independent of N throughout the bulk of the distribution. For any fixed position x such that the tail mass $T(|x|, t)$ remains $O(1)$ as $N \rightarrow \infty$, the weight scales as $w(x, t) \sim (NT(|x|, t))^{-\zeta}$, while the normalization factor behaves as $Z(t) \sim N^{-\zeta}$. The factors of N therefore cancel in the ratio $\alpha(x, t) = r w(x, t)/Z(t)$, yielding a well-defined, N -independent effective reset rate. Finite- N effects enter only through the extreme tail, where $T(|x|, t) \sim 1/N$ and the continuum description crosses over to the regime of extreme statistics. In the strict limit $N \rightarrow \infty$, this outer region is pushed to arbitrarily large $|x|$, and the age-structured equations become fully independent of N on all finite spatial scales.

Reduction to independent resetting ($\zeta = 0$)

For $\zeta = 0$ the rank-based weights are uniform,

$$w(x, t) \equiv 1, \quad (\text{S55})$$

so that the normalization factor reduces by mass conservation to

$$Z(t) = \int_{\mathbb{R}} C(x, t) dx = 1. \quad (\text{S56})$$

The effective reset rate is therefore spatially homogeneous,

$$\alpha(x, t) = r. \quad (\text{S57})$$

Substituting this into Eq. (S51) yields

$$\partial_t n(x, \tau, t) + \partial_\tau n(x, \tau, t) = -[\beta(\tau) + r] n(x, \tau, t), \quad (\text{S58})$$

with boundary condition (S53). This is exactly the age-structured equation for independent Poissonian resetting, recovered as the $\zeta = 0$ limit of the rank-based formulation.

Reduction to extremal resetting ($\zeta \rightarrow \infty$)

In the opposite limit $\zeta \rightarrow \infty$, the rank-based weight

$$w(x, t) = (1 + N T(|x|, t))^{-\zeta} \quad (\text{S59})$$

strongly suppresses resetting in the bulk. For any x such that $T(|x|, t) > 0$ one has $w(x, t) \rightarrow 0$, while only particles in the extreme tail, where $T(|x|, t) \simeq 0$, retain a nonvanishing weight. Consequently, the normalization factor $Z(t)$ is dominated by an $O(1/N)$ fraction of extreme particles and the effective reset rate vanishes in the bulk,

$$\alpha(x, t) \rightarrow 0 \quad \text{for bulk particles.} \quad (\text{S60})$$

Inside the support, Eq. (S51) therefore reduces to

$$\partial_t n(x, \tau, t) + \partial_\tau n(x, \tau, t) = -\beta(\tau) n(x, \tau, t), \quad (\text{S61})$$

which coincides with the bulk age-structured equation of the extremal-resetting protocol. Resetting acts only through the global constraint that the most distant particle is relocated to the origin, producing a compact support whose boundary is fixed self-consistently by mass conservation. Extremal resetting is thus recovered as the singular $\zeta \rightarrow \infty$ limit of the rank-based age-structure equations.

Steady state for $\beta > 1$

For $\beta > 1$, the mean waiting time is finite, see Eq. (S11), and a stationary state exists. At stationarity, Eq. (S51) reduces to

$$\partial_\tau n_s(x, \tau) = -[\beta(\tau) + \alpha(x)] n_s(x, \tau), \quad (\text{S62})$$

where the stationary effective reset rate is

$$\alpha(x) = r \frac{w(x)}{Z}, \quad Z = \int_{\mathbb{R}} w(x) C_s(x) dx. \quad (\text{S63})$$

The solution is

$$n_s(x, \tau) = n_s(x, 0) \Psi(\tau) e^{-\alpha(x)\tau}. \quad (\text{S64})$$

This has the same structure as Eq. (4) of the main text. Defining

$$\tilde{\mu}(\alpha) = \int_0^\infty \Psi(\tau) e^{-\alpha\tau} d\tau, \quad \hat{\psi}(\alpha) = \int_0^\infty \psi(\tau) e^{-\alpha\tau} d\tau, \quad (\text{S65})$$

we obtain

$$C_s(x) = n_s(x, 0) \tilde{\mu}(\alpha(x)), \quad J_s(x) = \frac{\hat{\psi}(\alpha(x))}{\tilde{\mu}(\alpha(x))} C_s(x), \quad (\text{S66})$$

where $J_s(x)$ is the stationary jump flux. Using the boundary condition (S53), the stationary density satisfies

$$\frac{C_s(x)}{\tilde{\mu}(\alpha(x))} = \int_{\mathbb{R}} \omega(x - x') \frac{\hat{\psi}(\alpha(x'))}{\tilde{\mu}(\alpha(x'))} C_s(x') dx' + r \delta(x). \quad (\text{S67})$$

Equation (S67) is a nonlinear, nonlocal integral equation for $C_s(x)$. The nonlocality originates from the jump kernel ω , while the nonlinearity arises from the self-consistent dependence of the reset rate $\alpha(x)$ on the tail mass $T(|x|)$ and hence on the density C_s itself. This reflects the collective nature of rank-based resetting: although the microscopic reset rule depends on global rank information, its manifestation appears through a spatially varying, density-dependent reset rate. In the limits $\zeta = 0$ and $\zeta \rightarrow \infty$, Eq. (S67) reduces to the linear integral equations corresponding to independent and extremal resetting, respectively. In the general case, analytical progress follows from exploiting the asymptotic separation between bulk and tail regions, as discussed below.

Large- $|x|$ behavior (tail)

We focus on the far-tail behavior $|x| \rightarrow \infty$ of the stationary density. This limit should be understood as follows: we first analyze the $N \rightarrow \infty$ description, for which $C_s(x)$ is smooth at fixed x , and only afterwards relate the resulting tail to finite- N extreme statistics.

As $|x| \rightarrow \infty$ the tail mass satisfies $T(|x|) \rightarrow 0$, hence

$$w(x) \rightarrow 1, \quad \alpha(x) \rightarrow \alpha_\infty = \frac{r}{Z}. \quad (\text{S68})$$

Using symmetry and the definition $T(s) = \int_{|y|>s} C_s(y) dy$, we may rewrite the normalization as

$$Z = \int_{\mathbb{R}} (1 + NT(|x|))^{-\zeta} C_s(x) dx = 2 \int_0^\infty (1 + NT(s))^{-\zeta} C_s(s) ds = \int_0^1 (1 + Nu)^{-\zeta} du, \quad (\text{S69})$$

where we used $dT/ds = -2C_s(s)$ so that $du = -2C_s(s) ds$. Evaluating the integral in Eq. (S69) gives

$$Z = \begin{cases} \frac{(1+N)^{1-\zeta} - 1}{N(1-\zeta)}, & \zeta \neq 1, \\ \frac{\log(1+N)}{N}, & \zeta = 1, \end{cases} \quad (\text{S70})$$

and therefore, for large N ,

$$\alpha_\infty = \frac{r}{Z} \sim \begin{cases} r(1-\zeta) N^\zeta, & \zeta < 1, \\ \frac{rN}{\log N}, & \zeta = 1, \\ r(\zeta-1) N, & \zeta > 1. \end{cases} \quad (\text{S71})$$

The qualitative change at $\zeta = 1$ reflects the transition in the large- N behavior of Z : for $\zeta > 1$ the integral is dominated by the extreme tail $u \sim 1/N$, whereas for $\zeta \leq 1$ finite- u contributions remain relevant.

In the far tail, where $\alpha(x) \simeq \alpha_\infty$ is effectively constant, Eq. (S67) becomes asymptotically linear. Using $(1 - \ell^2 \partial_x^2) \omega = \delta$ gives

$$\ell^2 g''(x) = (1 - \hat{\psi}(\alpha_\infty)) g(x), \quad g(x) = \frac{C_s(x)}{\tilde{\mu}(\alpha_\infty)}. \quad (\text{S72})$$

Thus

$$C_s(x) \sim A e^{-\kappa_\infty |x|}, \quad \kappa_\infty = \frac{1}{\ell} \sqrt{1 - \hat{\psi}(\alpha_\infty)}. \quad (\text{S73})$$

Importantly, at finite N , the edge of the distribution is set by $NT(|x|) \sim 1$, so the exponential tail $C_s(x) \sim e^{-\kappa_\infty |x|}$ implies $|x|_{\max} \sim \kappa_\infty^{-1} \log N$ (up to $O(1)$ corrections).

Bulk behavior

We now consider the stationary profile in the bulk, i.e. at fixed $|x| = O(1)$ as $N \rightarrow \infty$. Then $T(|x|) = O(1)$ and $w(x) \sim (NT(|x|))^{-\zeta} \sim N^{-\zeta}$, so that

$$\alpha_{\text{bulk}} = r \frac{w}{Z} \sim \begin{cases} O(1), & \zeta < 1, \\ O(1/\log N), & \zeta = 1, \\ O(N^{1-\zeta}), & \zeta > 1. \end{cases} \quad (\text{S74})$$

Thus, for $\zeta \geq 1$ the bulk reset rate vanishes as $N \rightarrow \infty$ (logarithmically at $\zeta = 1$), implying that renewal resetting becomes asymptotically ineffective in the bulk, while remaining strong in the far tail.

Starting from Eq. (S67), define

$$g(x) := \frac{C_s(x)}{\tilde{\mu}(\alpha(x))}, \quad q(x) := \hat{\psi}(\alpha(x)). \quad (\text{S75})$$

For $x \neq 0$ the injection term vanishes and Eq. (S67) becomes

$$g(x) = \int_{\mathbb{R}} \omega(x - x') q(x') g(x') dx'. \quad (\text{S76})$$

Applying $(1 - \ell^2 \partial_x^2)$ and using $(1 - \ell^2 \partial_x^2)\omega = \delta$ yields the exact local equation

$$\ell^2 g''(x) = [1 - q(x)] g(x), \quad x \neq 0, \quad (\text{S77})$$

where the nonlinearity is entirely contained in the self-consistent dependence $q(x) = \hat{\psi}(\alpha(x))$ with $\alpha(x) = r w(x)/Z$ and $w(x) = (1 + NT(|x|))^{-\zeta}$. Equation (S77) provides a convenient starting point for bulk approximations.

The regime $\zeta > 1$: extremal-like, piecewise linear core.

For $\zeta > 1$, Eq. (S74) implies that the effective reset rate $\alpha(x) = r w(x)/Z$ vanishes throughout the bulk as $N \rightarrow \infty$, $\alpha(x) = o(1)$ on $O(1)$ spatial scales. Since the waiting-time distribution has finite mean μ for $\beta > 1$, we may use the small- α expansion

$$\hat{\psi}(\alpha) = 1 - \mu\alpha + o(\alpha), \quad \tilde{\mu}(\alpha) \rightarrow \mu, \quad (\text{S78})$$

so that $q(x) = \hat{\psi}(\alpha(x)) \rightarrow 1$ in the bulk. Consequently, the exact local equation (S77) reduces to

$$g''(x) \simeq 0, \quad x \neq 0 \text{ in the bulk}, \quad (\text{S79})$$

and the leading-order bulk solution is piecewise linear,

$$g(x) \simeq a - b|x|. \quad (\text{S80})$$

The reset-induced injection at the origin does not generate a macroscopic δ -mass in this regime but instead enters through a discontinuity in the derivative of g at $x = 0$. Applying the operator $(1 - \ell^2 \partial_x^2)$ to the steady equation (S67) in the distributional sense yields the slope jump condition

$$g'(0^+) - g'(0^-) = -\frac{r}{\ell^2}. \quad (\text{S81})$$

For the even profile (S80), this fixes the slope as

$$b = \frac{r}{2\ell^2}. \quad (\text{S82})$$

The linear bulk approximation breaks down at large $|x|$, where the solution crosses over to a boundary layer and then to the exponential far tail derived above. The extent of the linear core, $|x| \lesssim L_N$, is determined implicitly by the extreme-statistics condition $NT(L_N) = O(1)$. Matching the bulk solution to the tail form

$$g_{\text{tail}}(x) \sim B e^{-\kappa_\infty |x|}, \quad \kappa_\infty = \frac{1}{\ell} \sqrt{1 - \hat{\psi}(\alpha_\infty)}, \quad (\text{S83})$$

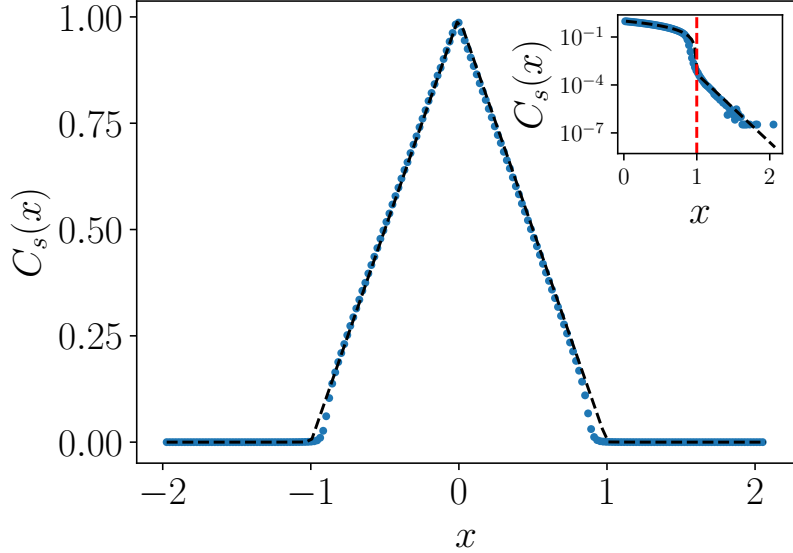


FIG. S1. Comparison between simulations and theoretical predictions for rank-based resetting in the stationary regime ($\beta = 1.5$, $\zeta = 2$). Symbols show the stationary spatial density $C_s(x)$ obtained from 5×10^4 independent realizations of an ensemble of $N = 10^4$ particles, which allows sampling of the far tail. Solid black lines indicate the theoretical bulk profile. Parameters are $\tau_0 = \ell^2 = 0.01$. Inset: semi-log plot highlighting the exponential decay of the tail and the agreement with theory up to finite-size corrections around $x \simeq L_N$. The dashed red line marks the approximate system size L_N predicted by the extremal-like bulk theory.

by continuity of g and g' at $|x| = L_N$ yields the effective boundary condition

$$a - bL_N \simeq \frac{b}{\kappa_\infty}, \quad \text{or equivalently} \quad a \simeq b(L_N + \kappa_\infty^{-1}). \quad (\text{S84})$$

This relation plays the same role as the endpoint condition in extremal resetting, with the exponential tail replacing the hard boundary of compact support.

Since the far-tail mass is $O(1/N)$, it is negligible in the normalization. Moreover, in this regime the stationary density is dominated by its regular bulk part, with no macroscopic δ -contribution at the origin. Using $C_s(x) \simeq \mu g(x)$ in the bulk and normalizing over the linear core gives

$$1 \simeq \int_{-L_N}^{L_N} \mu(a - b|x|) dx = 2\mu \left(aL_N - \frac{b}{2}L_N^2 \right). \quad (\text{S85})$$

Substituting (S82) and (S84), we obtain a closed equation for L_N ,

$$\frac{\mu r}{2\ell^2} \left(\frac{1}{2}L_N^2 + \frac{L_N}{\kappa_\infty} \right) \simeq 1 \quad \Rightarrow \quad L_N \simeq -\frac{1}{\kappa_\infty} + \sqrt{\frac{1}{\kappa_\infty^2} + \frac{4\ell^2}{\mu r}}. \quad (\text{S86})$$

In the regime $L_N \gg \kappa_\infty^{-1}$ this reduces to $L_N \simeq 2\ell/\sqrt{\mu r}$, recovering the extremal-resetting scaling.

In Fig. S1 we compare the theoretical bulk profile [Eqs. (S80)–(S86)] with numerical simulations, showing good agreement throughout the linear core and prediction of the effective system size L_N , including the onset of the exponential tail.

Importantly, for $\zeta < 1$, the effective reset rate remains $O(1)$ throughout the bulk in the large N limit, so that resetting is strong everywhere and the extremal-like reduction leading to a piecewise linear core no longer applies. In this regime the stationary equation for the bulk profile remains fully nonlinear and spatially nonlocal through the self-consistent dependence of $\alpha(x)$ on the tail mass. We therefore expect the bulk density to be controlled by a smooth, spatially varying balance between transport and renewal resetting. A natural starting point is a WKB-type approximation, in which the stationary profile is written as $C_s(x) \sim \tilde{\mu}(\alpha(x)) \exp[-S(x)]$ with $S'(x)$ determined locally by the effective reset rate. While such an approach captures the qualitative structure of the bulk for weak collective bias, a full self-consistent WKB analysis lies beyond the scope of the present work.

Time-dependent regime for $\beta < 1$

For $0 < \beta < 1$, the mean waiting time diverges and renewal processes exhibit aging. We analyze the consequences of rank-based resetting in this regime using the age-structured Eq. (S51) with boundary condition (S53).

Equation (S51) can be solved explicitly along characteristics. For $0 < \tau < t$ one finds

$$n(x, \tau, t) = n(x, 0, t - \tau) \Psi(\tau) \exp \left[- \int_{t-\tau}^t \alpha(x, s) ds \right], \quad (\text{S87})$$

where $\Psi(\tau) = \int_{\tau}^{\infty} \psi(s) ds$ is the survival probability of the underlying CTRW, as defined in the main text. Equation (S87) shows explicitly that the rank-based reset rate $\alpha(x, t)$ induces an exponential tempering of the heavy-tailed waiting-time distribution. For slowly varying $\alpha(x, t)$, this tempering acts as a local cutoff

$$\Psi_{\text{eff}}(\tau|x, t) \simeq \Psi(\tau) e^{-\alpha(x, t)\tau}, \quad (\text{S88})$$

with a characteristic cutoff time $\tau_c(x, t) \sim 1/\alpha(x, t)$. In the bulk, defined by fixed $|x| = O(1)$ as $N \rightarrow \infty$, the tail mass satisfies $T(|x|, t) = O(1)$ and the rank-based weight scales as $w(x, t) \sim N^{-\zeta}$. The normalization factor is dominated by the extreme tail for $\zeta \geq 1$, yielding $Z(t) \sim N^{-1}$ (up to logarithmic corrections at $\zeta = 1$). We therefore define the bulk reset rate as

$$\alpha_{\text{bulk}}(t) := \alpha(x, t) \Big|_{|x|=O(1)} \sim \begin{cases} O(1), & \zeta < 1, \\ O(1/\log N), & \zeta = 1, \\ O(N^{1-\zeta}), & \zeta > 1. \end{cases} \quad (\text{S89})$$

Considering the limit $N \rightarrow \infty$, for $\zeta \geq 1$, Eq. (S89) implies $\alpha_{\text{bulk}}(t) \rightarrow 0$, for $N \rightarrow \infty$, so that the effective cutoff time $t_c \sim 1/\alpha_{\text{bulk}}$ diverges. The exponential factor in Eq. (S87) thus becomes asymptotically ineffective in the bulk. As a result, the renewal dynamics are not truncated at long times, and the jump flux obeys the same asymptotic scaling as in the case of extremal resetting,

$$J(x, t) \simeq \lambda(t) C(x, t), \quad \lambda(t) \sim t^{\beta-1}, \quad (\text{S90})$$

reflecting persistent aging in the large N limit for $\zeta \geq 1$. As discussed in the main text, for any finite N , however, $\alpha_{\text{bulk}}(t)$ is strictly positive. Equation (S88) then implies a finite bulk cutoff time

$$t_c \sim \frac{1}{\alpha_{\text{bulk}}} \sim \begin{cases} \log N, & \zeta = 1, \\ N^{\zeta-1}, & \zeta > 1, \end{cases} \quad (\text{S91})$$

beyond which the algebraic decay of the renewal rate is suppressed. Thus, while the large N limit exhibits persistent aging for $\zeta \geq 1$, any finite system eventually crosses over to a regime controlled by the rank-based reset-induced cutoff.

S4: MONTE CARLO SIMULATIONS

We simulate N continuous-time random walkers on \mathbb{R} using an event-driven algorithm. Each particle i starts at $x_i(0) = 0$ and evolves via renewal waiting times and symmetric jumps:

1. Inter-jump times are i.i.d. draws from either (i) an exponential law with mean τ_0 , or (ii) a power-law (Pareto-type) law with survival function $\Pr(\tau > t) = (1 + t/\tau_0)^{-\beta}$ (scale $\tau_0 > 0$, tail exponent $\beta > 0$).
2. Given a jump event at time t , the position updates as $x_i(t^+) = x_i(t^-) + \Delta x$, where Δx is sampled from a symmetric jump kernel with scale parameter ℓ . We note here that in our simulations we have implemented Gaussian, two-sided exponential, and discrete ± 1 kernels. in the main text we showed results only for two-sided exponential kernel, but we have checked that none of our main results change when using a Gaussian kernel.

The simulation advances time by always executing the next scheduled event (a particle jump or a reset), selected by minimum time from a priority queue. After each jump, a new waiting time is drawn for that particle and its next jump is re-scheduled.

Resets occur according to an independent Poisson clock. At a reset time t_r , one particle is selected by a rule (below) and its position is instantaneously reset to the origin:

$$x_{i^*}(t_r^+) = 0.$$

The reset particle's next jump time is rescheduled according to the laws above. We implemented the three reset selection rules as follows:

1. Random reset: choose i^* uniformly from $\{1, \dots, N\}$.
2. Most-distant reset: choose $i^* = \arg \max_i |x_i(t_r^-)|$.
3. Rank-based reset: order particles by decreasing $|x_i(t_r^-)|$ to obtain ranks $k = 1, \dots, N$. Draw a rank k with probability $P(k) \propto k^{-\zeta}$; set i^* to that particle.

Implementation details. The simulator is implemented in modern C++ and exposed to Python via `pybind11`. An event-driven design with a binary heap efficiently maintains the next-event times for all particles and the reset clock, giving $O(\log N)$ updates per event. Preallocation and lightweight RNG usage enable large- N , long-time simulations with excellent performance.